Synthesis and characterization of diazine-ring containing hydrazones and their Zn(II) complexes

József Magyari[1,2], Berta Barta Holló[1], Marko V. Rodić[1], Imre Miklós Szilágyi[2], Katalin Mészáros Szécsényi[1]

[1] Department of Chemistry, Biochemistry and Environmental Protection, Faculty of Sciences, University of Novi Sad, 21000 Novi Sad, Trg Dositeja Obradovića 3, Serbia
[2] Department of Inorganic and Analytical Chemistry, Budapest University of Technology and Economics, H-1111 Budapest, Műegyetem rkp. 3, Hungary

ORCID numbers: József Magyari 0000-0002-9849-7689 ; Berta Barta Holló 0000-0002-5786-442X ; Marko V. Rodić 0000-0002-4471-8001 ; Imre Miklós Szilágyi 0000-0002-5938-8543 ; Katalin Mészáros Szécsényi 0000-0002-7494-7323

Corresponding author: Magyari József, dh.jozef.madjari@student.pmf.uns.ac.rs , tel.: +381691002959

Keywords: hydrazinophthalazine, hydralazine, pyridazine, dipyridyl ketone, Schiff base, zinc complexes

Abstract

Two new zinc(II) coordination compounds have been synthesized by the reaction of diazine-ring containing Schiff bases di(2-pyridyl) ketone phthalazine-1-hydrazone (*HzDPK*) and di(2-pyridyl) ketone 3-chloropyridazine-6-hydrazone (*HpDPK*) with zinc(II) salts in acetonitrile in the presence of triethylamine. The crystal and molecular structures of the complexes and that of the ligand *HpDPK* were determined by single-crystal X-ray structure analysis. In both complexes, zinc atoms are situated in distorted octahedral environments, formed by two meridionally coordinated NNN tridentate, mono-deprotonated ligands.

Since the applicability of the coordination compounds depends on their thermal properties, the thermal decomposition of the ligands and their complexes was followed by simultaneous TG–DSC measurements. The desolvation process of the complexes is rather slow as a consequence of a restricted diffusion through the lattice and finishes ~ 200 ˚C. The desolvated compounds are stable up to 340 ˚C. In order to follow the solvent evaporation and to have a better insight into the decomposition mechanism of the compounds coupled TG–MS measurements were carried out.

Introduction

Carcinogenesis underlies complex mechanisms and to address single target approaches is inadequate to prevent prevalence and deaths from the disease. The resistance of the human tumor to multiple chemotherapeutic drugs was recognized as one of the most important reasons for the failure of cancer therapy so it became a focus of cancer research. The phenomenon called multidrug resistance (MDR) subsequently appeared as a major impediment to the curative treatment of a variety of malignancies [1,2]. MDR caused by specific membrane transporters, such as ATP-binding cassette (ABC) or copper transporters, as well as other causes of drug resistance, hamper successful cancer chemotherapy [3]. Schiff bases can be involved in the prevention of MDR, besides, they show a broad range of biological activity, including analgesic, anti-inflammatory, antimicrobial, anti-tubercular, anticancer/antitumor, anticonvulsant, anti-diabetic and anti-hypertensive properties [4]. Some of them exhibit higher activity than the precursor drug [5]. Furthermore, their lower toxicity compared to hydrazines is also important [6]. Compounds with diazine [7] can be used also as precursors in the synthesis of new Schiff bases. One of them, 1-hydrazinophthalazine hydrochloride (*Hz·HCl*) was one of the first used vasodilators and still has been used in some urgent cases [8]. The hydrazino group plays a key role in its reactivity *in vivo* [9] and *in vitro* environment, too. Hydrazinophthalazine itself is a chelating, practically

bidentate ligand and with metal ions forms five-membered metallocycles [10]. The other diazine compound with less bulky structure, 3-chloro-6-hydrazinopyridazine (*Hp*), has comparable coordinational properties. Both contain hydrazino group which in the reaction with carbonyl compounds give Schiff bases.

One of the possibilities to enhance the pharmacological potency of biologically active compounds is their complexation with metals [11]. Some diazine-hydrazone coordination compounds which exhibited remarkable antiproliferative effect have already been synthesized by our group [12] so, the design, synthesis and characterization of similar Schiff base type ligands and their metal complexes make this topic promising for the further research.

In this work, we present the synthesis of two Schiff base type ligands, di(2-pyridyl) ketone phthalazine-1-hydrazone (*HzDPK*) and di(2-pyridyl) ketone 3-chloropyridazine-6-hydrazone (*HpDPK*) and their new zinc(II) complexes. The structures of the *HpDPK* ligand and the complexes were determined by single crystal X-ray diffraction method and confirmed by FT-IR, molar conductivity and thermal measurements, too. The desolvation of the complexes and the decomposition mechanism of the compounds were evaluated using data obtained by coupled TG–MS measurements.

Experimental

Materials

1-hydrazinophthalazine hydrochloride (*Hz·HCl*), 3-chloro-6-hydrazinopyridazine (*Hp*), di(2-pyridyl) ketone (*DPK*) and acetonitrile were from Sigma-Aldrich and used as received.

Preparation of the ligands

Di(2-pyridyl) ketone phthalazine-1-hydrazone (*HzDPK*)

In 50 cm^3 round-bottom flask *Hz·HCl* (7 mmol, 1.38 g) was dissolved by heating in 30 cm^3 EtOH : H_2O = 1 : 1 mixture. Di(2-pyridyl) ketone, *DPK***,** (7 mmol, 1.29 g) was dissolved in 5 cm^3 EtOH and combined with the initial solution. The reaction mixture was refluxed for 1.5 h, then solid $LiOAc{\cdot}2H_2O$ (7.35 mmol, 750 mg) was added to it and continued the reflux for further 30 minutes. The hot mixture was transferred into a beaker and cooled down to room temperature. The formed precipitate was separated by filtration through a fritted glass funnel, washed with 3 cm^3 EtOH and twice by water (5 cm^3) and dried on air. Yield: 2.0 g, 88 %.

Di(2-pyridyl) ketone 3-chloropyridazine-6-hydrazone (*HpDPK*)

In 25 cm^3 round-bottom flask *Hp* (5 mmol, 723 mg) was dissolved by gently heating in 6 cm^3 MeCN. Di(2-pyridyl) ketone, *DPK***,** (5 mmol, 921 mg) was dissolved in 4 cm^3 MeCN and combined with the initial solution. The reaction mixture was refluxing 2.5 h. The hot mixture was transferred into a beaker and cooled down to room temperature. The formed precipitate was filtered off, washed with 3 cm^3 MeCN and air dried. Yield: 1.2 g, 77.23 %.

The X-ray quality crystals have been obtained by slow evaporation of acetone : methanol = 1 : 1 solution of *HpDPK*.

Preparation of the complexes

Bis(di(2-pyridylketone)phthalazine-1-hydrazone)zinc(II), $[Zn(HzDPK–H)_2]{\cdot}CHCl_3$

In 100 cm^3 round-bottom flask *HzDPK* (1 mmol, 326 mg) was dissolved in 30 cm^3 MeCN by heating. Triethylamine (1 mmol, 0.14 cm^3), then $Zn(OAc)_2{\cdot}2H_2O$ (0.5 mmol, 110 mg) dissolved in 5 cm^3 MeCN was combined with the ligand solution. The reaction mixture was refluxed 2 h, ~~then, it was~~ cooled down to room temperature. The resulted orange coloured precipitate was separated by filtration. The precipitate was dissolved by stirring in 15 cm^3 MeCN + 25 cm^3 chloroform mixture. The solution was filtered off through a small pore size fritted glass funnel. The liquid phase was transferred into a 100 cm^3 Erlenmeyer-flask which was after sealed by perforated parafilm. After one week, dark-orange single crystals were formed and separated by filtration. Yield: 156 mg, 37.34 %.

Bis(di(2-pyridylketone)3-chloropyridazine-6-hydrazone)zinc(II), *[Zn(HpDPK–H)$_2$]·CHCl$_3$*

In 50 cm^3 round-bottom flask *HpDPK* (1 mmol, 311 mg) was dissolved in 10 cm^3 MeCN by heating, Triethylamine (1 mmol, 0.14 cm^3), then Zn(NO$_3$)$_2$·6H$_2$O (0.5 mmol, 149 mg) dissolved in 3 cm^3 MeCN was combined with the ligand solution. The reaction mixture was refluxed 1 h then it was cooled down to room temperature. The resulted orange coloured precipitate was separated by filtration. The precipitate was dissolved by stirring in 10 cm^3 MeCN + 20 cm^3 chloroform mixture, then filtered off through a small pored-sized fritted glass funnel. The solution was transferred into a 100 cm^3 Erlenmeyer-flask which was after sealed by perforated parafilm. After one week, dark-orange single crystals were formed and separated by filtration. Yield: 148 mg, 36.81 %.

Measurement methods

IR data were collected on a Thermo Nicolet Nexus 670 FT-IR spectrometer at room temperature in the range of 4000–400 cm^{-1} with resolution of 4 cm^{-1} using KBr pellets.

The molar conductivity of freshly prepared $1 \cdot 10^{-3}$ mol dm^{-3} solutions of the complexes in N,N-dimethylformamide (DMF) was determined at room temperature using a digital conductivity meter (Jenway 4510).

Thermal data were collected using TA Instruments SDT Q600 thermal analyser coupled to Hiden Analytical HPR-20/QIC mass spectrometer. The decomposition was followed from room temperature to 550 °C at 10 °C min^{-1} heating rate in nitrogen carrier gas (flow rate = 50 cm^3 min^{-1}). Sample holder / reference: alumina crucible / empty alumina crucible. Sample mass ~ 4 mg. Selected ions between *m/z* = 1–120 were monitored in Multiple Ion Detection Mode (MID).

Single crystal X-ray diffraction experiments were carried out at 295 K with Mo *Kα* radiation using a Gemini S diffractometer (Oxford Diffraction). For *HpDPK*, empirical absorption correction using spherical harmonics was performed with the *CRYSALIS PRO* [13]. For *[Zn(HpDPK–H)$_2$]·CHCl$_3$* and *[Zn(HzDPK–H)$_2$]·CHCl$_3$*, analytical numeric absorption correction using a multifaceted crystal model, followed by empirical absorption correction using spherical harmonics, has been applied. Structures were solved with the *SHELXT* [14] and refined with the *SHELXL* [15]. Carbon bonded hydrogen atom parameters were refined using a riding model, while nitrogen bonded hydrogen atom in *HpDPK* was freely refined with isotropic displacement parameter. The *SHELXLE* [16] was used as a graphical user interface for refinement procedures. Structures were validated by using Cambridge Structural Database (CSD) [17] and *Mercury CSD* [18]. The crystallographic data for *[Zn(HzDPK–H)$_2$]·CHCl$_3$*, *Hp* and *[Zn(HpDPK–H)$_2$]·CHCl$_3$* and have been deposited with the Cambridge Crystallographic Data Centre as Supplementary Publication No. CCDC 1568439 , CCDC 1568440 and CCDC 1568441, respectively. Molecular graphics were produced by *ORTEP* for Windows [19].

A disorder of CHCl$_3$ molecule is observed in the structure of *[Zn(HpDPK–H)$_2$]·CHCl$_3$*. To achieve reasonable geometry of disordered molecules, ADP and distance restraints were applied. The specimen of *[Zn(HzDPK–H)$_2$]·CHCl$_3$* was a non-merohedral twin, with 180° rotation around *c** axis as a twin law. The Bragg reflection intensities were measured in a full-sphere of reciprocal space in the range $2\theta < 52.6°$, with a total of 29574 reflections collected, 22691 of which are overlapped and 6883 isolated. Structure solution was obtained by processing 18556 reflections belonging to twin component 1 in HKLF4 format using *SHELXT* (among these, 15123 were overlapped reflections, the intensities of which were determined by deconvolution). For the final refinement cycles, 29574 reflections were merged to 11935 reflections in HKLF5 format.

Crystallographic and refinement details of *HpDPK*, *[Zn(HpDPK–H)$_2$]·CHCl$_3$* and *[Zn(HzDPK–H)$_2$]·CHCl$_3$* are shown in Table 1.

Table 1 Crystallographic and refinement details of HpDPK, $[Zn(HpDPK–H)_2]·CHCl_3$ and $[Zn(HzDPK–H)_2]·CHCl_3$

	HpDPK	$[Zn(HpDPK–H)_2]·CHCl_3$	$[Zn(HzDPK–H)_2]·CHCl_3$
Chemical formula	$C_{15}H_{11}ClN_6$	$C_{30}H_{20}Cl_2N_{12}Zn·CHCl_3$	$C_{38}H_{26}N_{12}Zn·CHCl_3$
M_r	310.75	804.22	835.44
Crystal system	Orthorhombic	Monoclinic	Triclinic
Space group	*Pbca*	$P2_1/c$	$P\bar{1}$
a / Å	14.4624(5)	13.7149(2)	10.4401(5)
b / Å	11.4369(3)	25.1743(7)	11.0460(6)
c / Å	17.2563(5)	20.0693(5)	17.2978(10)
α / °	90	90	81.733(5)
β / °	90	95.2972(18)	85.159(4)
γ / °	90	90	70.045(5)
V / Å^3	2854.27(15)	6899.6(3)	1854.22(18)
Z	8	8	2
μ / mm^{-1}	0.273	1.14	0.93
Crystal shape	Prism	Prism	Irregular
Colour	Off-white	Orange	Orange
Crystal size / mm	0.68 × 0.22 × 0.14	0.69 × 0.21 × 0.13	0.57 × 0.33 × 0.13
T_{min}, T_{max}	0.92, 1	0.716, 0.863	0.697, 0.894
Measured reflections	16572	45514	29574
Independent reflections	3521	15996	11935
Observed reflections	2686	10994	9909
R_{int}	0.025	0.031	0.034
θ range / °	2.7–29.0	2.5–29.0	2.4–29.1
$(\sin\theta/\lambda)_{max}$ / Å^{-1}	0.683	0.682	0.685
R [$F^2 > 2\sigma(F^2)$]	0.038	0.053	0.038
wR (F^2)	0.092	0.137	0.098
S	1.03	1.02	1.06
Parameters	203	883	534
Restraints	0	0	56
$(\Delta/\sigma)_{max}$	0.001	0.001	0.001
$\Delta\rho_{max}$, $\Delta\rho_{min}$ / e Å^{-3}	0.21, −0.21	1.03, −0.79	0.31, −0.35

Results and discussion

The ligands have been synthesized as free bases. By concerning the diazine ring, each ligand can be present in two prototropic tautomeric forms (Figure 1). As the single crystal X-ray diffraction measurement confirmed that *Hz·HCl* exists in the diazine ring in –NH tautomeric form [20] it was expected to keep it in its Schiff base *HzDPK*, too.

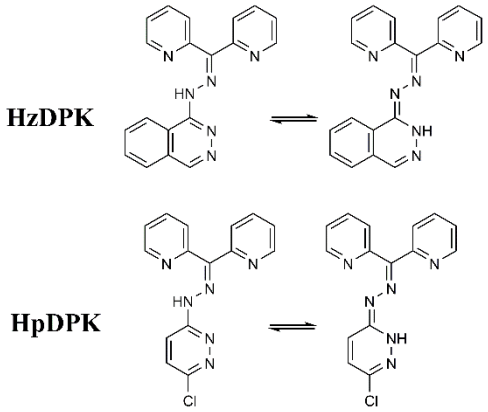

Figure 1 Prototropic tautomerism of the ligands

To assure the targeted coordinating properties of the ligands in the reaction with zinc(II) salts triethylamine as base was applied which led to the formation of neutral *bis*-ligand metal complexes with deprotonated ligands. MeCN/$CHCl_3$ solvent mixture found to be the best for obtaining X-ray quality single crystals. Complexes were crystallized in the form of chloroform solvates. As all the free nitrogen atoms in the complexes have tertiary character, the hydrogen bond formation is not possible.

Crystal and molecular structures

The *HpDPK* molecule (Figure 2) significantly deviates from planarity due to twisting of the pyridine rings in order to avoid steric clashes. The magnitude of the twisting is best perceived through torsion angles and τ(N3–C6–C1–N1) = 10.2(2), and τ(N3–C6–C7–N2) = −138.41(13)°. The reason for unequal magnitudes of twisting is the involvement of N1 atom in hydrogen bonding interaction with N4–H4A fragment of the hydrazone group. Geometrical parameters of this interaction are: N4···N1 = 1.946(18) Å, N4–H4A = 0.888(18) Å, H4A···N1 = 2.6263(18) Å, N4–H4A···N1 = 132.1(16)°. Additionally, the valence angles around C6 significantly deviate from ideal values, so that angle N3–C6–C1 equals 127.21(12)° and N3–C6–C7 angle is 111.68(11)°. These peculiar geometrical parameters are also observed for some structurally related di-2-pyridyl-ketone hydrazones [21–23]. The ^{1}H NMR spectrum is in accordance with the *HpDPK* molecular structure and the observed hydrogen bonding, too (Supplementary Material, Figure S1).

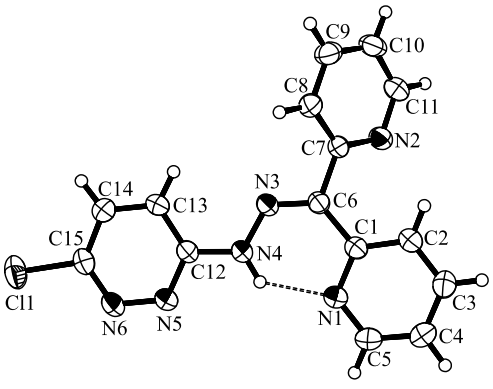

Figure 2 Molecular structure of *HpDPK* with atom numbering scheme

Molecular structures of *[Zn(HpDPK−H)$_2$]·CHCl$_3$* and *[Zn(HzDPK−H)$_2$]·CHCl$_3$* are depicted in Figure 3 furthermore, the selected structural parameters are given in Table 2. The asymmetric unit of *[Zn(HpDPK−H)$_2$]·CHCl$_3$* complex comprises two independent complex molecules and two $CHCl_3$ molecules, while the asymmetric unit of the complex *[Zn(HzDPK−H)$_2$]·CHCl$_3$* consists of a complex molecule and a disordered $CHCl_3$ molecule. Zinc atoms in both complexes are situated in distorted octahedral environments, formed by two meridionally coordinated NNN tridentate ligands. The amount of distortion may be appreciated

by measuring dihedral angles between two chelate planes (defined as plane through three donor atoms belonging to one ligand), which for *[Zn(HzDPK−H)$_2$]·CHCl$_3$* equals 83.80(10)°, and for *[Zn(HpDPK−H)$_2$]·CHCl$_3$* equals 85.72(11)° and 86.41(11)°, for two independent molecules, respectively. Also, distorted octahedral geometry is further evidenced by deviation of all the angles within coordination sphere from ideal geometries (trans valence angles are given in Table 2).

Ligands are coordinated through pyridine (N1), azomethine (N3) and diazine (N5) nitrogen atoms, thus forming two fused five-membered metallacycles. The metallacycles show a high degree of planarity, with the exception of Zn1–N1A–C1A–C6A–N3A ring in the complex *[Zn(HpDPK−H)$_2$]·CHCl$_3$*, which has envelope conformation with N3A as the pivot atom. Metal-ligand bond lengths are within expected values, with a notable trend that nitrogen atom N5 contribute to the shortest bond, and nitrogen atom N1 contribute to the longest bond within the coordination sphere.

The lengths of chemically equivalent bonds between the metal atom and ligator atoms belonging to two coordinated ligands, except of the bonds involving pyridine nitrogen N1, are in agreement within ca. 0.02 Å. In [Zn(HpDPK−H)$_2$]·CHCl$_3$, the difference between Zn1–N1A and Zn1–N1B bond lengths is ca. 0.03 Å (2.223(3) and 2.168(2) Å), while the difference between Zn2–N1D and Zn2–N1C bond lengths is ca. 0.05 Å (2.185(3) and 2.153(3) Å). Thus, Zn1–N1A and Zn2–N1D bonds are significantly longer compared to the rest of the bonds of the coordination polyhedron. On the other hand, in *[Zn(HzDPK−H)$_2$]·CHCl$_3$* the Zn1–N1A and Zn1–N1B bond lengths are by far the longest bonds in the coordination polyhedron (2.258(3) and 2.281(3) Å, respectively).

The CSD contains the structural data for three previously reported octahedral Zn(II) complexes with structurally related 1-hydrazinophthalazine and 3-chloro-6-hydrazinopyridazine based Schiff bases, refcodes: DITQOO [24] FARCEI [25] and CAJJAB [26]. In DITQOO and FARCEI structures, coordination mode of the tridentate ligands is analogous to that of *HpDPK*, while in CAJJAB both nitrogen atoms of the pyridazine ring are involved in coordination, thus forming a bridge between two metal atoms.

Intra ligand bond lengths have typical values for sp^2 hybridized atoms and are in accordance with the literature data [24–26]. The N3–C6 and N6–C15 bonds have lengths that correspond to localized double bonds. By inspection of structures of related compounds in the CSD, it is evident that in 1-hydrazinophthalazine based Schiff bases the hydrogen atom is located within pyridazine ring on nitrogen atom N5, while in 3-chloropyridazine-6-hydrazone based Schiff bases the hydrogen atom is located within hydrazone group at nitrogen atom N4 (which is in accordance with the structure of HpDPK). The ligands *HpDPK* and *HzDPK* are coordinated in monoanionic forms, and they are deprotonated at different positions. However, the negative charge in both cases is delocalized within C12–N5 and C12–N4 bonds, which eventually leads to the equivalent structure of their N4–C12–N5–N6 fragments.

From the comparison of intra-ligand bond lengths in *[Zn(HpDPK−H)$_2$]·CHCl$_3$* and in *HpDPK*, it can be seen that the most significant consequences of the monoanionic coordination form are shortening of N4–C12 and elongation of N5–C12 and N5A–N6 bonds, while for the rest of the ligand molecule only subtle changes are observable.

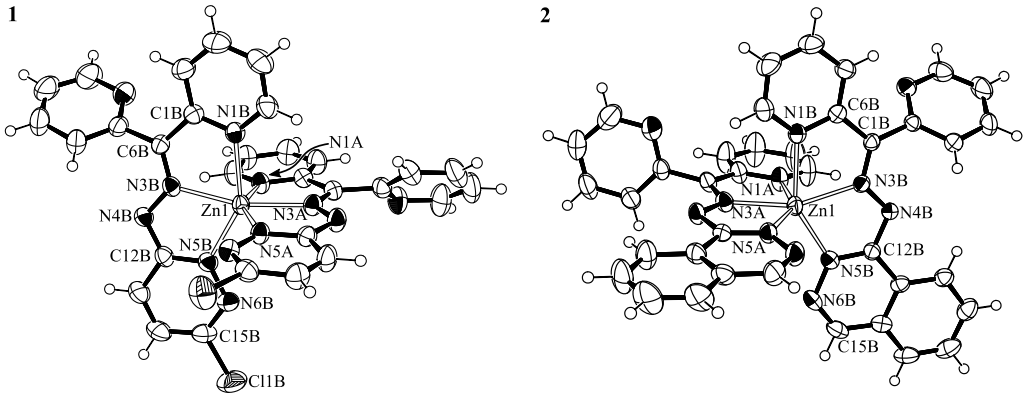

Figure 3 Molecular structures of ***[Zn(HpDPK−H)$_2$]·CHCl$_3$*** (**1**) and *[Zn(HzDPK−H)$_2$]·CHCl$_3$* (**2**) with selected atom numbering scheme. In case of *[Zn(HpDPK−H)$_2$]·CHCl$_3$* only one independent molecule is shown. Atoms

belonging to the other independent molecule are numbered in analogues way, with suffixes C and D for two coordinated ligand molecules. Solvent molecules are omitted for clarity.

Table 2 Selected bond lengths and bond angles of $[Zn(HpDPK{-}H)_2]\cdot CHCl_3$ (**1**), $[Zn(HzDPK{-}H)_2]\cdot CHCl_3$ (**2**) and HpDPK.

Bond	Bond length / Å			Bonds	Bond angle / °	
	1	**2**	HpDPK		**1**	**2**
Zn1–N1A	2.223(3)	2.281(3)		N1A–Zn1–N5A	147.52(10)	146.15(10)
Zn1–N1B	2.168(2)	2.258(3)		N1B–Zn1–N5B	148.19(9)	147.22(10)
Zn2–N1C	2.153(3)	–		N1C–Zn2–N5C	146.62(11)	–
Zn2–N1D	2.185(3)	–		N1D–Zn2–N5D	147.74(10)	–
Zn1–N3A	2.145(2)	2.138(3)		N3A–Zn1–N3B	164.78(10)	156.28(10)
Zn1–N3B	2.137(2)	2.136(2)		N3C–Zn2–N3D	166.72(10)	–
Zn2–N3C	2.159(3)	–				
Zn2–N3D	2.145(3)	–				
Zn1–N5A	2.110(3)	2.083(2)				
Zn1–N5B	2.105(2)	2.102(3)				
Zn2–N5C	2.096(3)	–				
Zn2–N5D	2.114(3)	–				
N3A–C6A	1.290(4)	1.297(4)	1.2989(17)			
N3B–C6B	1.301(4)	1.297(4)	–			
N3C–C6C	1.301(4)	–	–			
N3D–C6D	1.298(4)	–	–			
N3A–N4A	1.355(4)	1.355(4)	1.3442(16)			
N3B–N4B	1.355(3)	1.344(3)	–			
N3C–N4C	1.352(4)	–	–			
N3D–N4D	1.353(4)	–	–			
N4A–C12A	1.356(4)	1.359(4)	1.3737(18)			
N4B–C12B	1.358(4)	1.357(4)	–			
N4C–C12C	1.364(5)	–	–			
N4D–C12D	1.362(4)	–	–			
N5A–C12A	1.347(4)	1.336(4)	1.3266(18)			
N5B–C12B	1.339(4)	1.342(4)	–			
N5C–C12C	1.342(4)	–	–			
N5D–C12D	1.344(4)	–	–			
N5A–N6A	1.361(4)	1.371(4)	1.3465(17)			
N5B–N6B	1.358(3)	1.369(4)	–			
N5C–N6C	1.353(4)	–	–			
N5D–N6D	1.361(3)	–	–			
N6A–C15A	1.294(5)	1.289(5)	1.3072(19)			
N6B–C15B	1.298(4)	1.303(5)	–			
N6C–C15C	1.305(4)	–	–			
N6D–C15D	1.298(4)	–	–			
Cl1A–C15A	1.737(4)	–	1.7323(14)			
Cl1B–C15B	1.739(3)	–	–			
Cl1C–C15C	1.736(4)	–	–			
Cl1D–C15D	1.736(3)	–	–			

The molar conductivity values of the complexes in DMF referred to their non-electrolyte type which is in agreement with the structures: *[Zn(HpDPK−H)$_2$]·CHCl$_3$* λ_M = 11,35 Scm^2 mol^{-1}; *[Zn(HzDPK−H)$_2$]·CHCl$_3$* λ_M = 6,15 Scm^2 mol^{-1}.

FT-IR characterization

Due to complex formation, the νC=N and νC_{Ar}–N bands in the spectra of the complexes are shifted to lower frequencies compared to those in the ligands (Table 3). The complexes have been obtained in the form of chloroform solvate but due to the high volatility of $CHCl_3$ even at room temperature, it cannot be unambiguously detected in their IR spectra.

Table 3 Characteristic IR bands of the ligands and the complexes [Zn(HpDPK−H)$_2$]·CHCl$_3$ (**1**), [Zn(HzDPK−H)$_2$]·CHCl$_3$ (**2**)

Vibration	Wavenumber / cm^{-1}			
	HpDPK	**1**	HzDPK	**2**
ν C=N	1581–1426	1588–1400	1403	1395–1376
ν C_{Ar}-N	1321	1311	1321–1282	1317–1275
δ ring, δ C=N	1130–1023	1118–1023	1163–1049	1154–1045

Thermal analysis

Simultaneous TG – DSC measurements

As the thermal properties of new compounds often limit the practical applicability [27–33], the ligands and the corresponding zinc(II) complexes were thermally characterized. In Figure 4 the DTG curves of the ligands and the corresponding complexes are presented. DTG patterns show that the ligands have been obtained in a solvate-free form. The *HzDPK* has a relatively high thermal stability and starts to decompose at 239 °C DTG onset. The decomposition takes place in two main overlapping steps to 416 °C and afterwards slows down. *HpDPK* decomposes in a seemingly one-step process in the temperature range of 230 – 322 °C. The successive decomposition of the *HzDPK* can be explained by the separated fragmentation of the bulky, condensed-type phthalazine ring.

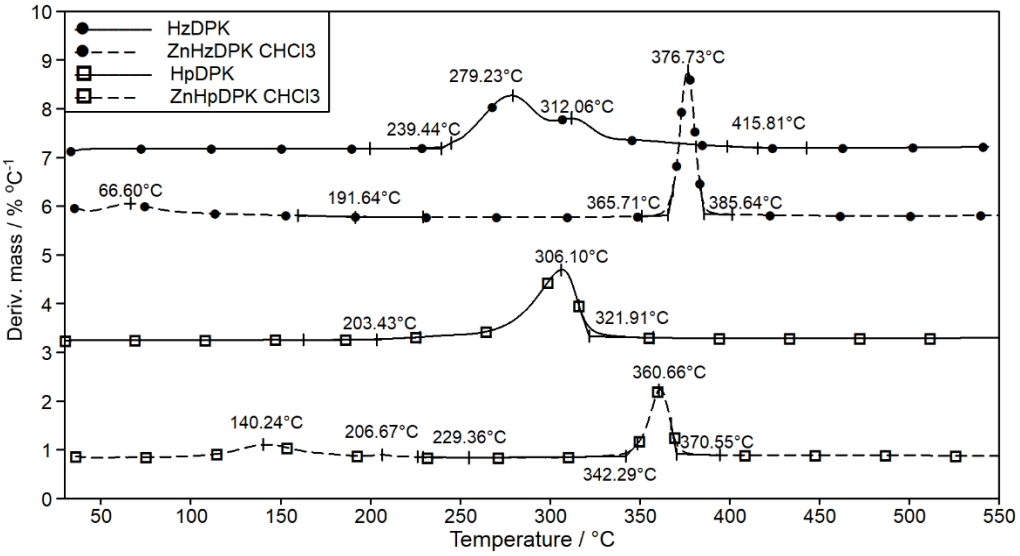

Figure 4 DTG curves of the ligands and the complexes. For the sake of clarity, the curves are shifted compared to zero.

The sharp endothermic peaks on the DSC curves refer to the melting of the ligands (Figure 5) The melting peak (t_{peak} =245.6 °C) of *HzDPK* is immediately followed by its decomposition (t_{peak} = 283.8 °C). *HpDPK* melts at much lower temperature (t_{peak} = 144.3 °C) and remains stable up to DSC onset 281 °C.

Both the complexes have been obtained as chloroform solvates and lose solvate even at room temperature (Figure 4). This phenomenon is more characteristic for *[Zn(HzDPK–H)$_2$]·CHCl$_3$* where the desolvation process occurs in a single step at lower temperatures (t_{peak} = 66.6 °C). The evaporation temperature of $CHCl_3$ in *[Zn(HpDPK–H)$_2$]·CHCl$_3$* is significantly higher. It occurs in two overlapping steps (t_{peak} = 140.2 °C and 206.7 °C) as a consequence of its restricted diffusion through the crystal lattice. The measured and the calculated solvent mass loss in *[Zn(HpDPK–H)$_2$]·CHCl$_3$* match within the experimental error (found 15.1 %; calc. 14.84 %). In a freshly prepared *[Zn(HzDPK–H)$_2$]·CHCl$_3$* the agreement between the calculated and the measured mass loss is not so good (found 15.6 %; calc. 14.29 %).

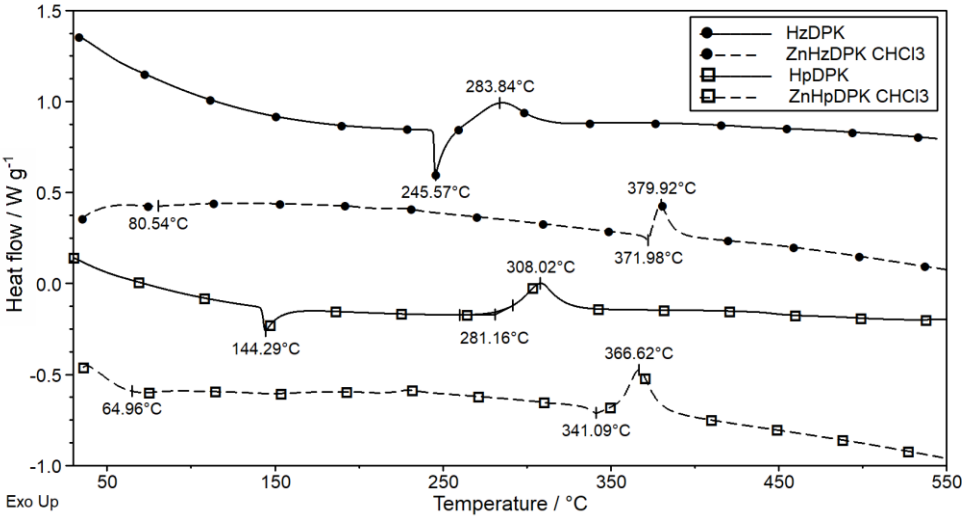

Figure 5 DSC curves of the ligands and the complexes. For the sake of clarity, the curves are shifted compared to zero

TG – MS measurements

Coordination compounds often crystallize with solvent. However, during storage or transport the solvent might be lost or replaced by water [34]. In these cases, the data obtained by TG – MS measurements give crucial data for the purity check by elemental analysis. TG – MS measurements were carried out to check the solvate evaporation of the complexes and to determine the decomposition processes of all the compounds. The characteristic *m/z* fragments of *HzDPK* decomposition process are shown in Figure 6. The *m/z* = 16, 17 and 18 fragments most probably refer to the evolution of NH_2^+, NH_3^+ and NH_4^+ in changing proportions. Fragment *m/z* = 30, in the accordance with structure of the compound, can be assigned to methylamine (CH_3NH_2), *m/z* = 32 to hydrazine (N_2H_4) and *m/z* = 44 to ethylamine ($C_2H_5NH_2$).

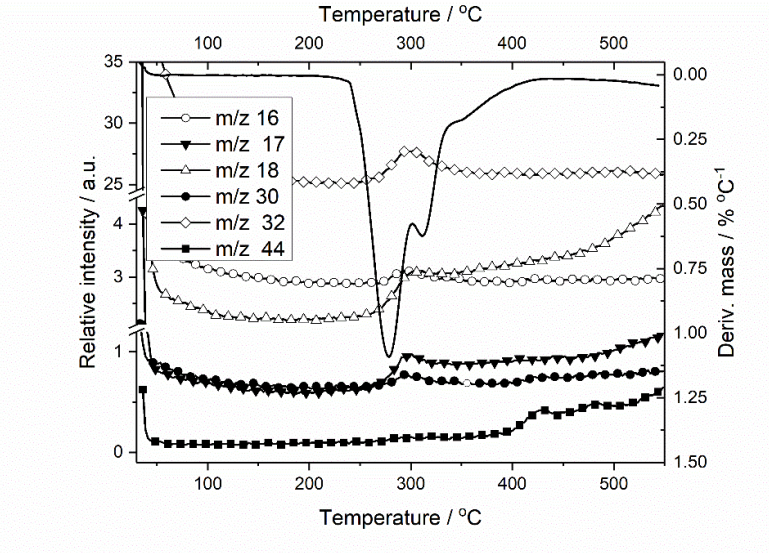

Figure 6 Selected fragments in the MS spectrum evolved during the thermal decomposition of *HzDPK*

HpDPK thermal decomposition fragments are presented in Figure 7 with the same *m/z* assignments.

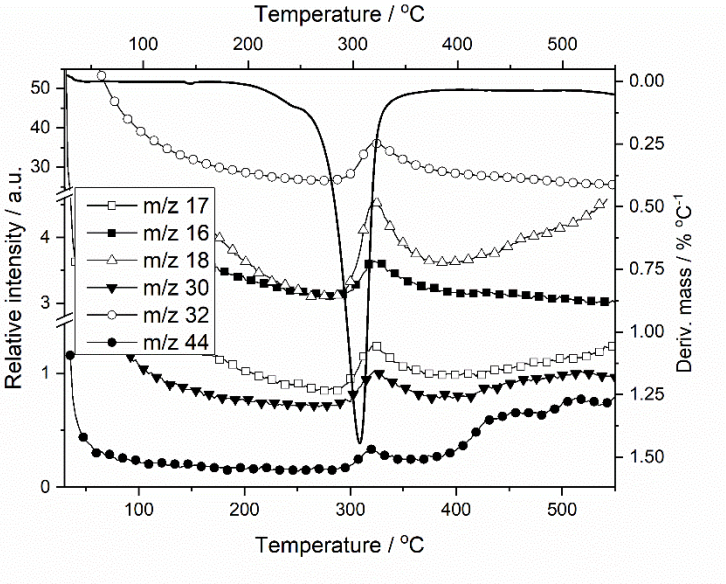

Figure 7 Selected fragments in the MS spectrum evolved during the thermal decomposition of *HpDPK*

The presence of the $CHCl_3$ solvent has been confirmed in both complexes. In contrast to the ligands, during the decompositions of the complexes, pyridine as a fragment can also be detected in the MS spectra.

The characteristic fragments of *[Zn(HzDPK–H)$_2$]·CHCl$_3$* are shown in Figure 8. Fragments *m/z* = 83 and *m/z* = 18 below ~ 200 °C belong to chloroform solvate and water, respectively. The change in the relative intensities of the *m/z* = 16, 17 and 18 signals at higher temperatures (~390 °C) refers to formation of NH_2^+, NH_3, NH_4^+, respectively, *m/z* = 44 to ethylamine ($C_2H_5NH_2$), while *m/z* = 79 to pyridine (C_5H_5N).

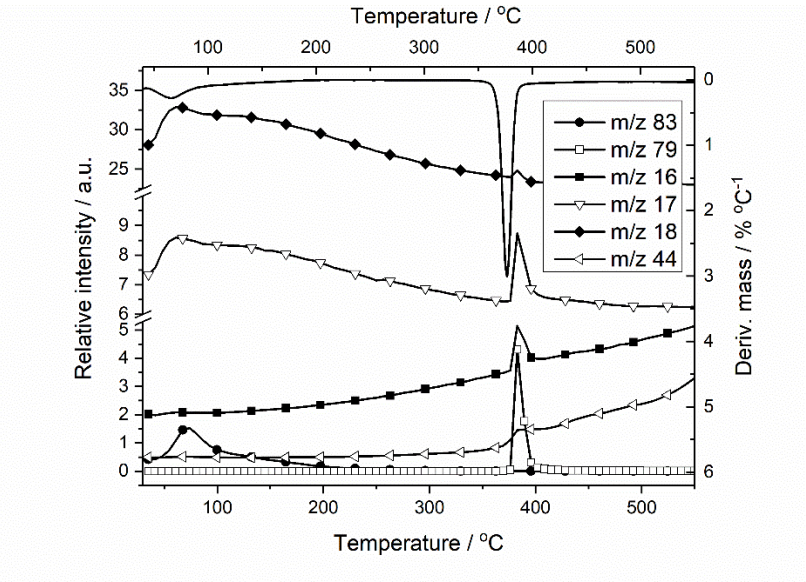

Figure 8 Selected fragments in the MS spectrum evolved during the thermal decomposition of *[Zn(HzDPK-H)$_2$]·CHCl$_3$*

In *[Zn(HpDPK–H)$_2$]·CHCl$_3$*, (Figure 9) the chloroform MS peak (*m/z* = 83) follow the DTG pattern. As the previous complex, it also contains adsorbed water (*m/z* = 17, 18). Beside, at the temperatures above the onset temperature of the desolvated product's decomposition signals for NH_2^+–NH_4^+ (*m/z* = 16, 17, 18), ethylamine ($C_2H_5NH_2$; *m/z* = 44), and pyridine (C_5H_5N; *m/z* = 79) appear.

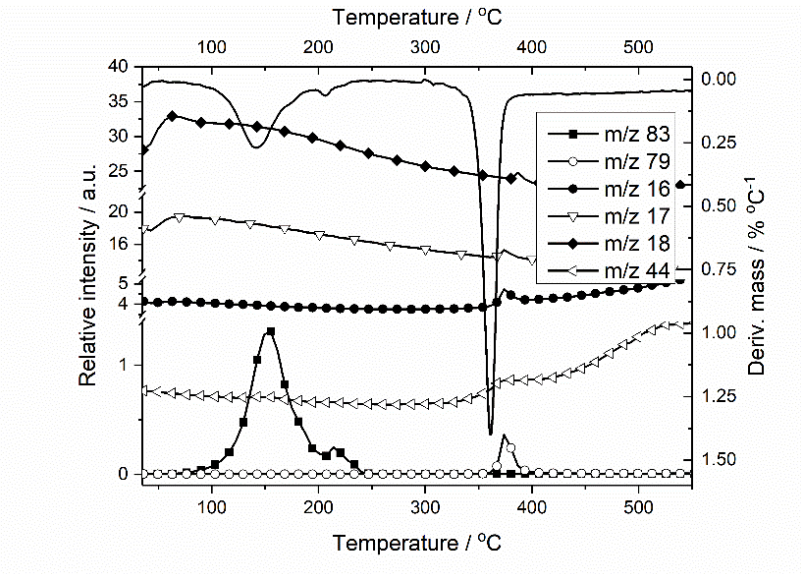

Figure 9 Selected fragments in the MS spectrum evolved during the thermal decomposition of *[Zn(HpDPK-H)$_2$]·CHCl$_3$*

Summary

Di(2-pyridyl)-ketone phthalazine-1-hydrazone (*HzDPK*), di(2-pyridyl)-ketone-3-chloropyridazine-6-hydrazone (*HpDPK*) and their new bis-ligand zinc(II) complexes, *[Zn(HzDPK-H)$_2$]·CHCl$_3$* and *[Zn(HpDPK-H)$_2$]·CHCl$_3$* were synthesized and characterized by single crystal X-ray diffraction, infrared spectroscopy (FT-IR), thermal analysis and coupled TG–MS measurements.

According to single crystal X-ray analysis, *HpDPK* contains intramolecular hydrogen bond which was proved by NMR measurement, too (See Supporting Information). Zinc atoms in both complexes are situated in a distorted octahedral environment, formed by two meridionally coordinated NNN tridentate, mono-deprotonated ligands. Ligands are coordinated through pyridine, azomethine and diazine nitrogen atoms, thus forming two fused five-membered metallacycles. FT-IR spectra of the complexes show the coordination of the ligands as the characteristic bands are shifted to lower frequencies. By TGA and TG–MS measurements the solvent content of the complexes was evaluated. It was found that chloroform partially evaporates during the storage and in part is replaced by water molecules. The desolvated coordination compounds have a significantly higher thermal stability than the corresponding ligands. All compounds practically decompose in one step giving small fragments which mainly belong to ammonia. Fragments with a higher *m/z* ratio belong to pyridine or alkylamines.

Acknowledgements

This research was supported by Ministry of Education, Science and Technological Development of the Republic of Serbia (Grant no. 172014). József Magyari gratefully acknowledges Hungarian Academy of Sciences (MTA) Domus Hungarica Grant for the research support.

References

1. Housman G, Byler S, Heerboth S, et al. Drug Resistance in Cancer: An Overview. Cancers. 2014;6:1769-1792.
2. Zilahi G, Artigas A, Martin-Loeches I. What's new in multidrug-resistant pathogens in the ICU? Ann Intensive Care. 2016;6:96-106
3. Locher KP. Mechanistic diversity in ATP-binding cassette (ABC) transporters. Nat Struct Mol Biol. 2016;23:487–493.
4. Kumar J, Rai A, Raj V. A Comprehensive Review on the Pharmacological Activity of Schiff Base Containing Derivatives. Org Med Chem IJ. 2017;1:555564.
5. Popiołek Ł. Hydrazide-hydrazones as potential antimicrobial agents: Overview of the literature since 2010. Med Chem Res. 2017;26:287–301.
6. Verma G, Marella A, Shaquiquzzaman M, Akhtar M, Ali MR, Alam MM. A review exploring biological activities of hydrazones. J Pharm Bioallied Sci. 2014;6:69–80.
7. Azab ME, Rizk SA, Mahmoud NF. Facile Synthesis, Characterization, and Antimicrobial Evaluation of Novel Heterocycles, Schiff Bases, and N-Nucleosides Bearing Phthalazine Moiety. Chem Pharm Bull. 2016;64:439–50.
8. Cohn JN, McInnes GT, Shepherd AM. Direct-acting vasodilators. J Clin Hypertens (Greenwich). 2011;13:690–2.
9. Nelson M-AM, Baba SP, Anderson EJ. Biogenic Aldehydes as Therapeutic Targets for Cardiovascular Disease. Curr Opin Pharmacol. 2017;33:56–63.
10. Al-Falahi H, May PM, Roe AM, Slater RA, Trott WJ, Williams DR. Metal binding by pharmaceuticals. Part 4. A comparative investigation of the interaction of metal ions with hydralazine, prizidilol and related compounds. Agents Actions. 1984;14:113–20.

11. Abu-Dief AM, Mohamed IMA. A review on versatile applications of transition metal complexes incorporating Schiff bases. Beni-Suef University Journal of Basic and Applied Sciences. 2015;4:119–33.
12. Barta Holló B, Magyari J, Armaković S, Bogdanović GA, Rodić MV, Armaković SJ, et al. Coordination compounds of a hydrazone derivative with Co(III), Ni(II), Cu(II) and Zn(II): Synthesis, characterization, reactivity assessment and biological evaluation. New J Chem. 2016;40:5885–95.
13. Rigaku Oxford Diffraction. CrysAlisPro Software system, version 1.171.38.46. Rigaku Corporation, Oxford, UK; 2015. 2015. Rigaku Corporation.
14. Sheldrick GM. SHELXT - Integrated space-group and crystal-structure determination. Acta Crystallogr Sect A Found Adv. 2015;71:3–8.
15. Sheldrick GM. Crystal structure refinement with *SHELXL*. Acta Crystallogr Sect C Struct Chem. 2015;71:3–8.
16. Hübschle CB, Sheldrick GM, Dittrich B. ShelXle: A Qt graphical user interface for *SHELXL*. J Appl Crystallogr. 2011;44:1281–4.
17. Groom CR, Bruno IJ, Lightfoot MP, Ward SC. The Cambridge Structural Database. Acta Crystallogr Sect B Struct Sci Cryst Eng Mater. 2016;72:171–9.
18. Macrae CF, Bruno IJ, Chisholm JA, Edgington PR, McCabe P, Pidcock E, et al. Mercury CSD 2.0 - new features for the visualization and investigation of crystal structures. J Appl Crystallogr. 2008;41:466–70.
19. Farrugia LJ. *WinGX* and *ORTEP for Windows*: An update. J Appl Crystallogr. 2012;45:849–54.
20. Okabe N, Fukuda H, Nakamura T. Structure of hydralazine hydrochloride. Acta Crystallogr C Cryst Struct Commun. 1993;49:1844–5.
21. Bakir M, Conry RR, Green O. Polymorphic di-2-pyridyl ketone 4-nitrophenylhydrazone (dpknph): The structure of [beta]-dpknph. Acta Crystallogr Sect C Cryst Struct Commun. 2005;61:607–609.
22. Bakir M, Green O. Di-2-pyridyl ketone p-aminobenzoyl-hydrazone hydrate. Acta Crystallogr Sect C Cryst Struct Commun. 2002;58:263–265.
23. Swearingen JK, Kaminsky W, West DX. Structural and spectral studies of di-2-pyridyl ketone 3-piperidyl- and 3-hexamethyleneiminylthiosemicarbazone and their cobalt(II), nickel(II) and copper(II) complexes. Transit Met Chem. 2002;27:724–31.
24. Deng W-T, Liu J-C, Cao J. Syntheses, crystal structures and properties of four new coordination polymers involving a schiff base ligand bearing an easily abstracted proton in the hydrazone backbone. Inorg Chem Commun. 2013;35:315–7.
25. Grünwald KR, Volpe M, Cias P, Gescheidt G, Mösch-Zanetti NC. Pyridazine-versus pyridine-based tridentate ligands in first-row transition metal complexes. Inorg Chem. 2011;50:7478–88.
26. Goldberg AE, Kiskin MA, Popov LD, Levchenkov SI, Shcherbakov IN, Tupolova YP, Kogan VA. Crystal structure of a trinuclear complex of zinc(II) with 2,6-Di-tert-butyl-p-quinone 1'-phthalazinylhydrazone. J Struct Chem. 2014;55:475–80.
27. Di Foggia M, Bonora S, Tinti A, Tugnoli V. DSC and Raman study of DMPC liposomes in presence of Ibuprofen at different pH. J Therm Anal Calorim. 2017;127:1407–17.
28. Li C-H, Jiang Y, Jiang J-H, Li X, Xiao S-X, Tao L-M, et al. Standard molar enthalpy of formation of [(C12H8N2)2Bi(O2NO)3] and its biological activity on Schizosaccharomyces pombe. J Therm Anal Calorim. 2017;128:1743–51.
29. Saad FA, Elghalban MG, Al-Fahemi JH, Yarkandy N, El-Metwaly NM, Abou-Melha KS, et al. Simulative aurintricarboxylic acid molecular docking with antitumor activity for its VO(II), Cr(III), Mn(II) and Fe(III) complexes, HF/DFT modeling and elaborated EPR studies. J Therm Anal Calorim. 2017;128:1565–78.
30. Srivastva U, Malhotra RK, Kaushik SC. Review of heat transport properties of solar heat transfer fluids. J Therm Anal Calorim. 2017;130:605–21.
31. Krisyuk VV, Sysoev SV, Turgambaeva AE, Nazarova AA, Koretskaya TP, Igumenov IK, Morozova NB. Thermal behavior of methoxy-substituted Pd and Cu β-diketonates and their heterobimetallic complex. J Therm Anal Calorim. 2017;130:1105–10.
32. Abd El-Halim HF, Omar MM, Anwar MN. Preparation, characterization, antimicrobial and anticancer activities of Schiff base mixed ligand complexes. J Therm Anal Calorim. 2017;130:1069–83.
33. Begović NN, Vasić MM, Blagojević VA, Filipović NR, Marinković AD, Malešević A, Minić DM. Synthesis and thermal stability of cis-dichloro[(E)-ethyl-2-(2-((8-hydroxyquinolin-2-il)methylene)hidrazinyl)acetate-κ2 N]-palladium(II) complex. J Therm Anal Calorim. 2017;130:701–11.
34. Jaćimović ŽK, Giester G, Kosović M, Bogdanović GA, Novaković SB, Leovac VM, Latinović N, Barta Holló B, Mészáros Szécsényi. Solvent exchange reactions in coordination compounds. J Therm Anal Calorim (2017) 127:1501–1509

1
2